


RESEARCH ARTICLE | MAY 17 2023

Bubble growth and departure behavior in subcooled flow boiling regime

Nikhil Chitnavis ; Harish Pothukuchi ; B. S. V. Patnaik 

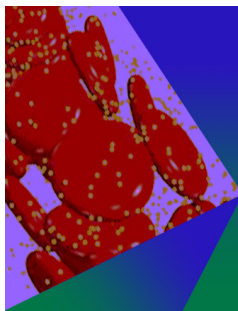


Physics of Fluids 35, 053327 (2023)

<https://doi.org/10.1063/5.0145889>



CrossMark



Physics of Fluids

Special Topic: Flow and Forensics

Submit Today!



Bubble growth and departure behavior in subcooled flow boiling regime

Cite as: Phys. Fluids **35**, 053327 (2023); doi: [10.1063/5.0145889](https://doi.org/10.1063/5.0145889)

Submitted: 8 February 2023 · Accepted: 1 May 2023 ·

Published Online: 17 May 2023



View Online



Export Citation



CrossMark

Nikhil Chitnavis,¹ Harish Pothukuchi,^{1,2} and B. S. V. Patnaik^{1,a)}

AFFILIATIONS

¹Department of Applied Mechanics, Indian Institute of Technology Madras, Chennai 600036, India

²Department of Mechanical Engineering, Indian Institute of Technology Jammu, Jammu 181221, India

^{a)}Author to whom correspondence should be addressed: bsvp@iitm.ac.in

ABSTRACT

Understanding the detailed dynamics of bubble ebullition cycle is central to effectively exploit coolant phase change in subcooled flow boiling. In the present study, the bubble growth rate and the bubble departure mechanism in subcooled flow boiling conditions are investigated. The bubble growth rate is estimated by employing an energy balance model, which ensures that the applied wall heat flux contribution to components, such as (i) microlayer evaporation, (ii) conduction through superheated layer region, and (iii) condensation heat transfer, are accounted. The bubble departure diameter and the type of departure (i.e., sliding or lift-off) are predicted using a simple force balance model on the vapor bubble. The implemented models are thoroughly validated against the benchmark experimental data. Furthermore, the influence of operating conditions, viz., pressure (1–3 bar), mass flux (200–1000 kgm⁻²s⁻¹), heat flux (200–500 kWm⁻²), and the degree of subcooling (20–30 K) on the bubble dynamics, is investigated for subcooled flow boiling conditions. Based on the parameters considered, a flow regime map is developed to identify the bubble departure type and diameter for a given set of operating conditions. It was noticed that the bubble departure diameter was maximum at low pressure (1 bar), low mass flux (200 kgm⁻²s⁻¹), high heat flux (500 kWm⁻²), and low degree of subcooling (20 °C). For all the values of pressure and degree of subcooling, the sliding mode of departure was noticed at low and high mass flux values, whereas bubble departs by lift-off for moderate values of mass flux.

Published under an exclusive license by AIP Publishing. <https://doi.org/10.1063/5.0145889>

I. INTRODUCTION

Coolant phase change yields higher heat transfer rates in the form of latent heat without any temperature rise. Therefore, flow boiling heat transfer is highly sought after in a wide spectrum of fluid-thermal systems, viz., heat exchangers, steam generators, etc. However, higher the vapor phase volume fraction near the heated surface, lower the heat transfer rate. This may be primarily attributed to the poor heat transfer characteristics of vapor phase. Therefore, the advantage of phase change can be exploited only by achieving controlled phase change phenomenon, which aims at maintaining the bulk liquid temperature below the coolant saturation temperature—termed as subcooled flow boiling. In this regime, the vapor bubbles are formed at the preferred nucleation sites on the heated surface when the wall superheat is adequate to trigger the coolant phase change. The formed vapor bubbles grow to a maximum size, called bubble departure diameter, to depart from the respective nucleation sites on the heated surface. The bubble departure from the heated surface can take place in two different modes, viz., (i) bubble lifts off normal to the heated surface or (ii) bubble slides along the heated surface. The bubble

departure size plays a significant role in determining the rate of heat transfer from the heated surface. It should be noted that smaller the departure diameter, larger the heat transfer from the heated surface. Therefore, an accurate prediction of the bubble growth rate, and departure diameter, and its frequency is very much essential.

A number of experimental studies have been dedicated to understanding both pool boiling¹ as well as flow boiling.² Recently, hydrophilic surfaces have been used to investigate the influence of subcooling and the associated dry patch dynamics.³ On the numerical front, volume of fluid (VOF) based interface tracking approaches⁴ have been used in the computational fluid dynamics (CFD) calculations. Apart from traditional finite volume based approaches, the aspects of liquid–vapor phase change has been studied using methods such as lattice Boltzmann.^{5,6} However, in phase change, vapor bubble formation, its growth rate, and departure diameter from the heated surface are important.^{7–10} Klausner *et al.*⁷ have performed experiments to predict the bubble departure diameter for saturated flow boiling conditions with mass flux of 112–287 kg s⁻¹ m⁻² and heat flux of 11–26 kWm⁻². They have observed that the primary mode of bubble

departure is by sliding along the heated surface and then the bubbles lift off. They have also proposed a force balance model for the first time to calculate the bubble departure diameter and validated it against their experimental data. Situ *et al.*⁸ conducted experiments to predict the bubble growth rate and departure diameter at 1 bar pressure, mass flux of 466–900 kg s⁻¹ m⁻², and heat flux of 60.7–206 kW m⁻². In their model, they have considered heat transfer from the superheated layer for the calculation of bubble radius [Eq. (1)] in conjunction with the force balance approach. Similarly, Du *et al.*¹¹ and Zuber¹² also used only the conduction model for the prediction of bubble size,

$$R_b(t) = \frac{2b}{\sqrt{\pi}} Ja \sqrt{\alpha_f t}. \quad (1)$$

Here, Ja represents Jakob number, which is defined as the ratio of sensible heat to the latent heat transferred to the coolant. R_b and α_f are the bubble radius and thermal diffusivity of fluid, respectively.

Sugrue *et al.*⁹ conducted experiments to investigate the influence of pressure and mass flux conditions on the bubble departure diameter by varying the angle of inclination of the heated plate. They concluded that with an increase in the inclination of the heated surface from 0° to 90°, a gradual decrease in bubble departure diameter was noticed. Bucci *et al.*¹⁰ have conducted pool boiling experiments and compared the force balance model against their experimental data. They have concluded that the force balance model is neither robust nor accurate for the prediction of bubble departure diameter. Experimental studies are conducted for the flow boiling of water at different operating conditions. By and large, all numerical models are based on energy and force balance on a vapor bubble, and most studies validated against their own experimental data for the prediction of vapor bubble growth rate and departure diameter. These bubble growth models, when coupled with the detailed computational fluid dynamics (CFD) simulations, are useful in predicting volume fraction distribution accurately.

The bubble growth rate for the flow boiling conditions is derived from the energy balance. Often the applied wall heat flux is compartmentalized and observed to be the summation of heat transfer components contributing to microlayer evaporation, superheated layer, and condensation,¹³

$$q_w = q_{ml} + q_{sl} + q_c, \quad (2)$$

where q_w is the total wall heat flux, q_{ml} , q_{sl} , and q_c represent heat transfer from microlayer evaporation, superheated layer, and due to condensation, respectively.

Although there are three components of heat transfer as described in Eq. (2), only heat transfer from microlayer or heat transfer from superheated layer or the combination of two modes of heat transfer are significantly used for the calculation of bubble growth rate depending on the operating conditions. Zhou *et al.*¹⁴ have developed a model for the bubble growth rate and validated it with the experimental data of both water and refrigerant by considering the conduction through superheated layer, microlayer evaporation, and condensation. They have estimated the bubble departure diameter by empirical correlation. Colombo and Fairweather¹⁵ accounted for all the three types of heat transfer, i.e., microlayer evaporation, conduction from superheated layer, and condensation in a subcooled liquid for the calculation of bubble diameter. However, they assumed the portion of bubble in contact with subcooled liquid as constant in their model. However, it is not easy to estimate the portion of bubble in contact with the subcooled liquid as

it will vary with the bubble radius during its growth. This issue was rectified by Raj *et al.*¹⁶ as the portion of bubble in contact with subcooled liquid is calculated by means of thermal boundary layer thickness.

Duhar *et al.*¹⁷ have studied the bubble growth in the near wall region in a shear flow by performing experiments as well as using the force balance model. In their force balance model, they have included the added mass force or unsteady drag force in both the x - (along the heated wall) and y - (normal to the heated wall) directions. However, they neglected the horizontal force balance (i.e., departure by sliding is ignored) by enforcing bubble departure to happen only by lift-off from the heated surface. Yoo *et al.*^{18,19} developed a novel mechanistic model for the prediction of growth rate of a sliding bubble and compared it with their own experimental results. This model is developed by modifying Ünal's model²⁰ for the prediction of bubble departure diameter. Unlike in Ünal's model,²⁰ Yoo *et al.*¹⁹ have considered a constant value for the bubble diameter for t (time) = 0. Legendre *et al.*²¹ have studied the lift, drag, and added mass forces on a sliding bubble (post its departure) in a linear shear flow. In their study, they have considered that the bubble slides along the heated wall with a velocity (U_b) in the direction of flow. van der Geld²² has also studied the dynamics of sliding bubble, but using a Lagrangian approach. They have ignored the fluid viscosity, but considered the effect of vorticity.

Zanje *et al.*²³ developed a one-dimensional saturated vapor model for the prediction of bubble growth by coupling mass, momentum, and energy conservation equations. Their coupled model is able to predict the bubble growth against the experimental data over the entire range of Ja varying from 15 to 2700. Park *et al.*²⁴ explained the bubble departure behavior by defining two subcategories as (i) ejecting bubble (directly lifts off from the nucleation site) and (ii) lifting-off bubble (slides along the heated wall for a distance from the nucleating site before lifting off). They studied the effect of mass flux and heat flux on the bubble diameter. Ahmadi *et al.*²⁵ experimentally observed the sliding and lifting behavior of bubbles for different pressure, mass flux, and heat flux conditions. They discussed the sliding and lift-off behavior of bubbles based on Ja . They have observed that for $Ja > 35$, bubbles lift off from the heated surface, whereas for $Ja < 35$, bubbles slide along the surface. For $15 < Ja < 35$, bubbles depart by sliding along the heated surface before lifting off into the bulk liquid.

From the brief literature discussed above, it can be understood that numerical models based on energy and force balance are widely employed to predict the bubble growth rate and the departure diameter.^{7–10} However, studies on characterizing the bubble departure behavior are very few. Furthermore, the models are very sensitive to the errors and may cause larger deviations in the prediction of bubble size.¹⁰ To this end, the present study focuses on extensive validation of the developed numerical model against the available experimental data. The effect of operating conditions such as pressure, mass flux, heat flux, and degree of subcooling on the bubble growth rate, its departure diameter and behavior is studied. Based on the validation studies and generated data, the present study classifies and develops a flow regime chart to identify the bubble departure diameter and the type of departure from the nucleation site. The present study also identifies the forces that are responsible for sliding or lifting off.

II. METHODOLOGY

To study the behavior of bubble growth and the bubble departure diameter in the flow boiling conditions, a bubble growth model based

on the energy balance and a force balance model are employed. This approach accounts for conduction, evaporation, and condensation, and various forces acting on the bubble.

A. Bubble growth model

The schematic of a vapor bubble on the vertical heated surface is shown in Fig. 1. The vapor bubble is assumed to be a growing sphere; in its growth phase, a liquid microlayer is formed as the liquid is trapped in the gap between the bubble and the heated wall. The temperature around the vapor bubble reaches a temperature slightly above the saturated temperature forming a superheated layer. When the bubble grows to a size greater than the superheated layer thickness, the top portion of the bubble is exposed to the subcooled bulk liquid, resulting in condensation heat transfer. In the bubble growth model, the applied wall heat flux is divided into three components, viz., conduction heat transfer through the superheated layer, microlayer evaporation, and condensation heat transfer from the portion of the bubble exposed to the subcooled bulk liquid. Considering the vapor bubble as a control volume, the energy balance for the growing bubble can be written as follows:

$$\dot{E}_{\text{stored}} = \dot{E}_{\text{in}} - \dot{E}_{\text{out}} + \dot{E}_{\text{gen}}. \quad (3)$$

As there is no heat generation within the bubble, $\dot{E}_{\text{gen}} = 0$. Hence, \dot{E}_{stored} is equal to the amount of heat transfer to the bubble (\dot{E}_{in}), i.e., the sum of microlayer evaporation and conduction heat

transfer through the superheated layer, and from the bubble (\dot{E}_{out}), i.e., condensation heat transfer from the top portion of the bubble in contact with the subcooled bulk liquid. Also, the stored energy is responsible for the bubble growth, which can be expressed in terms of latent heat of vaporization (h_{lv}). The conduction heat transfer through the superheated layer is estimated using

$$\dot{E}_{\text{in,conduction}} = \sqrt{\frac{3}{\pi}} \frac{k_l(T_o - T_{\text{sat}})}{\alpha^{0.5}} t^{-0.5} A_o. \quad (4)$$

The heat transfer due to microlayer evaporation is expressed as

$$\dot{E}_{\text{in,evaporation}} = Pr^{-0.5} [\rho_l C_{pl}(T_o - T_{\text{sat}}) \alpha^{0.5} A_{\text{eva}}]. \quad (5)$$

The condensation heat transfer from the bubble is expressed as

$$\dot{E}_{\text{out,condensation}} = h_{\text{cond}}(T_{\text{sat}} - T_{\text{bulk}}) A_{\text{cond}}. \quad (6)$$

Equations (4)–(6) are substituted in the energy balance equation (3) (Refs. 15 and 16) as follows:

$$\begin{aligned} \rho_l h_{lv} \frac{d(4/3\pi R_b^3)}{dt} = & \{ Pr^{-0.5} [\rho_l C_{pl}(T_o - T_{\text{sat}}) \alpha^{0.5} A_{\text{eva}}] \\ & + \sqrt{\frac{3}{\pi}} \frac{k_l(T_o - T_{\text{sat}})}{\alpha^{0.5}} t^{-0.5} A_o \\ & - h_{\text{cond}}(T_{\text{sat}} - T_{\text{bulk}}) A_{\text{cond}} \}. \end{aligned} \quad (7)$$

In Eq. (7), A_{eva} and A_o denote the areas that contributed for the heat transfer from the microlayer and superheated region, respectively. Dividing both sides of Eq. (7) with the surface area of the bubble ($A_{\text{bubble}} = 4\pi R_b^2$), A_o/A_{bubble} and $A_{\text{eva}}/A_{\text{bubble}}$ will appear in the equation. These area ratios represent the area covered by the microlayer and superheated region out of the total vapor bubble surface area. So, $A_{\text{eva}}/A_{\text{bubble}}$ will be simplified to a constant value $1/C$, where C is constant. A_o/A_{bubble} is written in terms of bubble portion covered by subcooled liquid $(1 - f)$. After simplification, the above equation is written as follows:

$$\begin{aligned} \frac{d(R_b)}{dt} = & \left(C^{-1} Pr^{-0.5} + \sqrt{\frac{3}{\pi}} (1 - f) \right) Ja \alpha^{0.5} t^{-0.5} \\ & - \frac{h_{\text{cond}}}{\rho_l h_{lv}} (T_{\text{sat}} - T_{\text{bulk}}) f, \end{aligned} \quad (8)$$

where Ja is Jakob number ($Ja = \frac{\rho_l C_{pl}(T_{\text{wall}} - T_{\text{sat}})}{\rho_g h_{lg}}$), α is the thermal conductivity of the fluid, and f is the portion of bubble in contact with the subcooled liquid. The value of C in Eq. (8) can vary from 0.8 to 1.2.²⁶ However, in the present study, this value is taken as 1.78.^{15,16} The condensation heat transfer coefficient (h_{cond}) is calculated using the Ranz and Marshal²⁷ correlation,

$$h_{\text{cond}} = \frac{k_l}{d_b} (2 + 0.6 Re_b^{0.5} Pr^{0.3}). \quad (9)$$

B. Wall temperature

The correlations of Chen²⁸ and Gungor and Winterton²⁹ are used for the calculation of wall temperature at constant heat flux. The correlations used in the wall temperature computation is presented in Table I. The calculated wall temperature from both the correlations are compared with Sugrue *et al.*⁹ (Fig. 2). It is observed that, there is

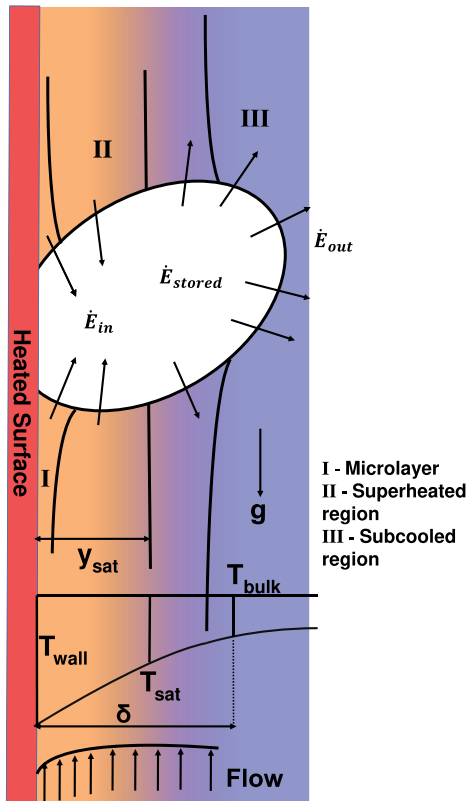


FIG. 1. Schematic of energy balance for a growing bubble in the bulk liquid.

TABLE I. Correlations used in wall temperature prediction.

Authors	Correlations
Chen ²⁸	$q'' = h_{\text{conv}}(T_{\text{wall}} - T_{\text{bulk}}) + h_{\text{nb}}(T_{\text{wall}} - T_{\text{sat}})$ $h_{\text{conv}} = 0.023 Re_l^{0.8} Pr^{0.4} \frac{k_l}{D_h} F$ $h_{\text{nb}} = 0.00122 \left(\frac{k_l^{0.79} C_{pl}^{0.45} \rho_l^{0.49}}{\sigma^{0.5} \mu_l^{0.29} h_{lv}^{0.24} \rho_g^{0.24}} \right) \Delta T_{\text{sat}}^{0.24} \Delta P^{0.75} S$ $F = 1 \text{ and } S = \frac{1}{1 + 2.53 \times 10^{-6} Re_{lp}^{1.17}}$
Gungor and Winterton ²⁹	$q'' = h_{\text{conv}} E (T_{\text{wall}} - T_{\text{bulk}}) + h_{\text{nb}} S (T_{\text{wall}} - T_{\text{sat}})$ $h_{\text{conv}} = 0.023 Re_l^{0.8} Pr^{0.4} \frac{k_l}{D_h}$ $h_{\text{nb}} = 55 P_r^{0.12} (-\log_{10} P_r)^{-0.55} M^{-0.5} q^{0.67}$ $E = 1 \text{ and } S = \frac{1}{1 + 1.15 \times 10^{-6} Re_{lp}^{1.17}}$

not a significant difference between the predictions of Chen²⁸ and Gungor and Winterton²⁹ correlations when compared with the experimental data.⁹ Hence, the correlation of Chen²⁸ is used for the prediction of wall temperature in the present numerical model.

1. Portion of bubble in contact with subcooled liquid

The portion of the bubble in contact with the subcooled liquid is difficult to calculate as the size of the bubble grows with time. However, for the present study, f (portion of bubble in contact with the subcooled liquid) is calculated using a linear correlation of temperature distribution, which varies from wall temperature to bulk temperature of the liquid.

For calculating the temperature distribution, the Kader's³⁰ model is used. The following equations are used for the calculation of the temperature profile:

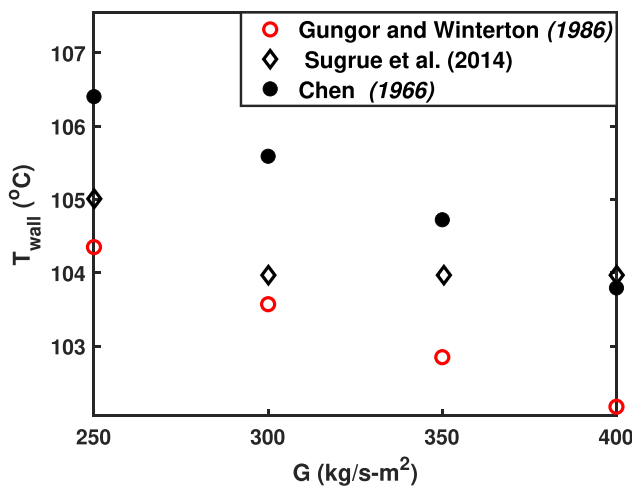


FIG. 2. Variation of wall temperature T_{wall} (°C) with mass flux G ($\text{kgm}^{-2}\text{s}^{-1}$), compared against the experimental studies of Sugrue *et al.*⁹

$$\frac{T_{\text{wall}} - T_l}{T_\tau} = Pr y^+ e^\tau + \left\{ 2.12 \ln \left[\frac{(1 + y^+) 2.5(2 - \bar{y})}{1 + 4(1 - \bar{y})^2} \right] + \beta(Pr) \right\} e^{-\frac{1}{\tau}}, \quad (10)$$

$$\tau = \frac{0.01(Pr y^+)^4}{1 + 5Pr^3 y^+} \quad T_\tau = \frac{q}{\rho_l C_{pl} u_*}, \quad (11)$$

$$\beta(Pr) = (3.85 Pr^{1/3} - 1.3)^2 + 2.12 \ln(Pr), \quad (12)$$

$$T_l = \begin{cases} T_{\text{bulk}} & \text{for } y = \delta \text{ or } \bar{y} = 1 \\ T_{\text{sat}} & \text{for } y = y_{\text{sat}}, \end{cases} \quad (13)$$

where, in Eq. (13), δ is the thermal boundary layer thickness measured from the heated surface to the point where the temperature of the fluid is equal to the bulk temperature. And y_{sat} is the distance measured from the heated surface to the point where the fluid temperature is equal to the saturation temperature of the fluid (T_{sat}). Both these distances from the heated surface are shown in Fig. 1.

Based on temperature distribution, y_{sat} and δ are determined, and the portion of the bubble in contact with the subcooled liquid is calculated as

$$f = 1 - \frac{y_{\text{sat}}}{\delta}. \quad (14)$$

C. Force balance on a growing vapor bubble

The representation of forces acting on the nucleating bubble in flow boiling conditions is shown in Fig. 3. The heated surface makes an inclination angle of θ with the horizontal, and gravity acts perpendicular to the horizontal in the downward direction. The force balance model is considered in two directions, viz., tangential and normal directions to the heated surface. The unbalanced force component causes the bubble to detach from the heated surface. If the cumulative value of forces is greater than zero in the tangential direction, the bubble departs from the heated surface by sliding along the heated wall. Whereas, if the cumulative value of forces is greater than zero in the normal direction, the bubble departs by lifting off from the heated

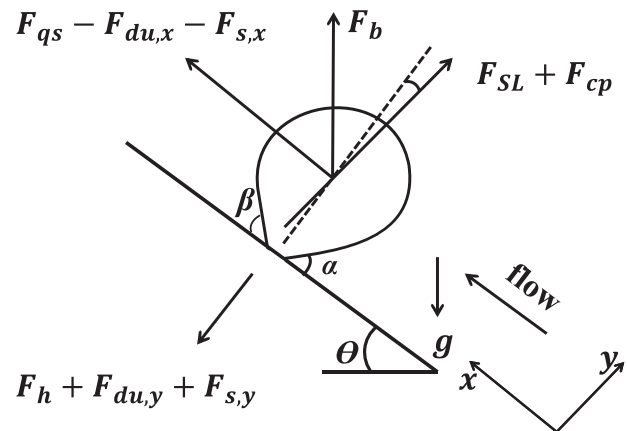


FIG. 3. Schematic representation of different forces acting on the vapor bubble.

surface. In both cases, the diameter with which the vapor bubble leaves its nucleation site is called as, bubble departure diameter. The forces that act on the bubble during its growth are discussed as follows.

1. Surface tension force

Surface tension force tries to oppose the detachment of the bubble against the drag and the force of buoyancy force. For the flow boiling condition, the bubble has two contact angles with the heated surface as shown in Fig. 3. Based on these contact angles, surface tension force is defined as follows:

$$F_{sx} = -1.25 d_w \sigma \frac{\pi(\alpha - \beta)}{\pi^2 - (\alpha - \beta)^2} (\sin \alpha - \sin \beta), \quad (15)$$

$$F_{sy} = -d_w \sigma \frac{\pi}{(\alpha - \beta)} (\cos \beta - \cos \alpha), \quad (16)$$

where F_{sx} and F_{sy} are the surface tension forces in the x - and y -directions, α and β are the advancing and receding contact angles, d_w is the bubble contact diameter with the wall. Following Raj *et al.*¹⁶ and Yun *et al.*,³¹ d_w is taken as $d_b/15$.

2. Shear lift force

This force acts on the bubble in the perpendicular direction of the heated surface. It tries to detach the bubble from the heated surface against the surface tension force. This shear lift force was given by Klausner *et al.*,⁷ which was based on the expression given by Mei and Klausner,³² and Auton.³³ The shear lift force is defined as follows:

$$F_{sl} = 0.5 \rho_l U_l^2 \pi R_b^2 \left[3.87 G_s^{0.5} (Re_b^{-2} + 0.118 G_s^2)^{0.25} \right], \quad (17)$$

$$G_s = \frac{dU_l R_b}{dy U_l}, \quad (18)$$

$$Re_b = \frac{\rho_l U_l d_b}{\mu_l}. \quad (19)$$

The fluid velocity near the wall is assumed as single phase turbulent velocity profile given by Situ *et al.*,⁸

$$u^+ = \frac{U_l}{u_*} = \frac{4}{\ln 5} (\ln y^+ + 1), \quad (20)$$

$$u_* = \sqrt{\frac{\tau_{wall}}{\rho_l}}, \quad (21)$$

where $y^+ = \frac{y u_*}{\nu_l}$, $\tau_{wall} = \frac{f_l \rho_l v_l^2}{8}$, and v_l is the area average velocity of the liquid, and f_l is the friction factor.

3. Unsteady drag force

The bubble, during its growth, pushes the surrounding liquid by exerting a force termed as added mass force or unsteady drag force. As this force varies with respect to time (as the bubble grows in size with time), it is called the unsteady drag force, which is also referred to as the added mass force.^{8,34} As the bubble grows, the bubble displaces the surrounding fluid, and, in the case of flow boiling, since the bubble tilts toward the flow direction, the force is asymmetrical. Therefore, a component of force is considered in both x - and in y -directions. Assuming

the bubble to be in hemispherical shape, this force can be calculated as follows:

$$F_{du} = -\rho_l \pi R_b^2 \left[R_b \ddot{R}_b + 1.5 \dot{R}_b^2 \right], \quad (22)$$

where R_b is the bubble radius, $\dot{R}_b = \frac{dR_b}{dt}$ and $\ddot{R}_b = \frac{d\dot{R}_b}{dt}$.

4. Quasi-static drag force

Quasi-static drag force is defined as the drag imparted by flow on the stationary body given by Mei and Klausner.³⁵ The drag force for the turbulent flow is defined as follows:

$$\frac{F_{qs}}{6\pi\mu_l U_l R_b} = \frac{2}{3} + \left[\left(\frac{12}{Re_b} \right)^n + 0.769^n \right]^{1/n}, \quad (23)$$

where $n = 0.65$.

5. Buoyancy force, contact pressure force, and hydrodynamic force

Buoyancy force arises due to difference in density inside and outside of the bubble. It acts in the vertically upward direction on the bubble perpendicular to the horizontal surface,

$$F_b = \frac{4}{3} \pi R_b^3 (\rho_l - \rho_g) g, \quad (24)$$

where ρ_l and ρ_g are the density of surrounding liquid and density of vapor in the bubble, respectively.

Contact pressure force arises due to the difference in pressure inside and outside of the bubble, which acts perpendicular to the heating surface. Hydrodynamic pressure also acts perpendicular to the heated surface. Both these forces were given by Klausner *et al.*⁷

$$F_{cp} = \frac{\pi d_w^2 2\sigma}{4r_r} \quad r_r \approx 5R_b, \quad (25)$$

$$F_h = \frac{9}{8} \rho_l U_l^2 \frac{\pi d_w^2}{4}. \quad (26)$$

Summation of the forces in x - and y -directions is as follows:

$$\sum F_x = F_{sx} + F_{qs} + F_{dux} + F_b \sin \theta, \quad (27)$$

$$\sum F_y = F_{sy} + F_{duy} + F_{sl} + F_h + F_{cp} + F_b \cos \theta. \quad (28)$$

The magnitude of the forces are dependent on the bubble size; thus, increase in the bubble size increases the magnitude of the forces. As a result of the increased magnitude of the forces, the vapor bubble tends to depart from the nucleation site in the direction of the resultant force. If $\sum F_x > 0$, then the bubble slides along the heated surface, or if $\sum F_y > 0$, then the bubble lifts off. In both the cases, either bubble slides or lifts off from the heated surface, and the corresponding bubble size is considered as the bubble departure diameter.

III. RESULTS AND DISCUSSION

In the present study, the bubble growth rate, departure diameter, and its behavior are predicted based on energy and force balance approach on the vapor bubble. The validation studies against the available experimental data are presented in this section. The bubble growth

TABLE II. Description of the experimental data chosen for validation studies.

	Prodanovic <i>et al.</i> ³⁶	Cao <i>et al.</i> ³⁷	Situ <i>et al.</i> ⁸	Sugrue <i>et al.</i> ⁹	Klausner <i>et al.</i> ⁷	Duhar <i>et al.</i> ¹⁷	Ahmadi <i>et al.</i> ²⁵
Fluid	Water	Water	Water	Water	R-113	N-pentane	Water
D_h (mm)	9.3	12	19.1	16.7	25	16.6	13.33
G (kgm ⁻² s ⁻¹)	76.6–766	143.7	466–900	250–400	112–287	18.91–80	325–1170
ΔT_{sub} (°C)	10–30	39.3	1.5–20	10–20	Saturated	Saturated	4–30
q (kWm ⁻²)	200–1000	185	60.7–206	50–100	11–26	...	81–611
Orientation	Vertical	Vertical	Vertical	0°–90°	Horizontal	Horizontal	Vertical

rate and departure diameters are predicted for the operating pressure (1–3 bars), inlet mass flux (200–1000 kgm⁻²s⁻¹), wall heat flux (200–500 kWm⁻²), and degree of subcooling ($\Delta T_{\text{sub}} = 20$ –30 °C).

A. Validation studies

The validation studies were performed by comparing the present model predictions against the experimental data.^{7–9,25,36,37} Table II contains the experimental data chosen for the validation of the present study. The chosen experimental studies include the data of water and R-113 refrigerant, $9.3 \leq d(\text{mm}) \leq 25$, $76.6 \leq G(\text{kgm}^{-2}\text{s}^{-1}) \leq 1170$, $11 \leq q(\text{kWm}^{-2}) \leq 1000$, and $0 \leq \Delta T_{\text{sub}}(\text{K}) \leq 39.3$ for different orientations. A bubble growth model caters to assessing various components of heat transfer, such as the microlayer conduction, evaporation, and condensation to estimate the growth of the vapor bubble before its departure. To predict the bubble departure diameter, the force balance model is coupled with the bubble growth model. Corresponding energy and force balance calculations are implemented in the MATLAB³⁸ environment. The bubble growth and bubble departure diameter predictions are compared against the experimental data listed in Table II for a range of operating conditions. The present model predictions for the bubble growth and the bubble departure diameter are obtained using two approaches. In the first approach (model 1), microlayer evaporation, conduction in superheated layer,

and condensation in subcooled liquid region are considered for predicting the bubble growth. Whereas in the second approach (model 2), conduction in the superheated layer is only considered for the calculation of bubble growth phase. Predictions from both the models are compared against the experimental data to identify the significant components of the heat transfer during the bubble growth.

The validation of the present numerical models is performed by comparing the bubble growth rate and the departure diameters. The numerical predictions of bubble growth is compared against the experimental data of Prodanovic *et al.*³⁶ and Cao *et al.*³⁷ by considering the two models. In Fig. 4, experiment data of Prodanovic *et al.*³⁶ are compared against the prediction model of Mikic *et al.*,³⁹ Du *et al.*,¹¹ and Colombo and Fairweather.¹⁵ As shown in Fig. 4, a good agreement with the experimental data is noticed, when model 1 is considered. However, bubble diameter is overpredicted when model 2 is considered. This is due to the higher values of bubble diameter corresponding to the conduction alone, as the bubble is considered to have grown completely within the superheated layer. The bubble diameter corresponding to the individual components of heat transfer is presented in Fig. 5. It should be noted that, for both the operating pressures of 1–3 bars, the bubble diameter corresponding to the microlayer evaporation and conduction in superheated layer contribute to the increase in bubble size. Whereas, the condensation component results in the decrease in bubble diameter; hence, it has to be treated with a negative

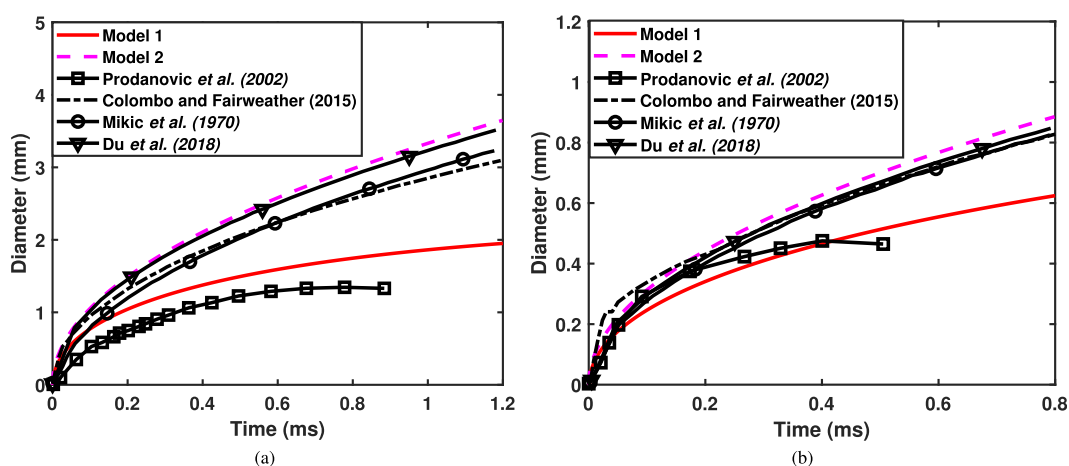


FIG. 4. Comparison of bubble growth rate against the experimental data of Prodanovic *et al.*³⁶ for (a) $p = 1$ bar, $G = 410.4 \text{ kgm}^{-2}\text{s}^{-1}$, and $q = 0.6 \text{ MWm}^{-2}$, and (b) $p = 3$ bar, $G = 391.7 \text{ kgm}^{-2}\text{s}^{-1}$, and $q = 0.6 \text{ MWm}^{-2}$. Results from the present study are plotted as model 1 and model 2. Model 1 accounts for all three effects (microlayer evaporation, conduction, and condensation), while model 2 refers to only the conduction effect.

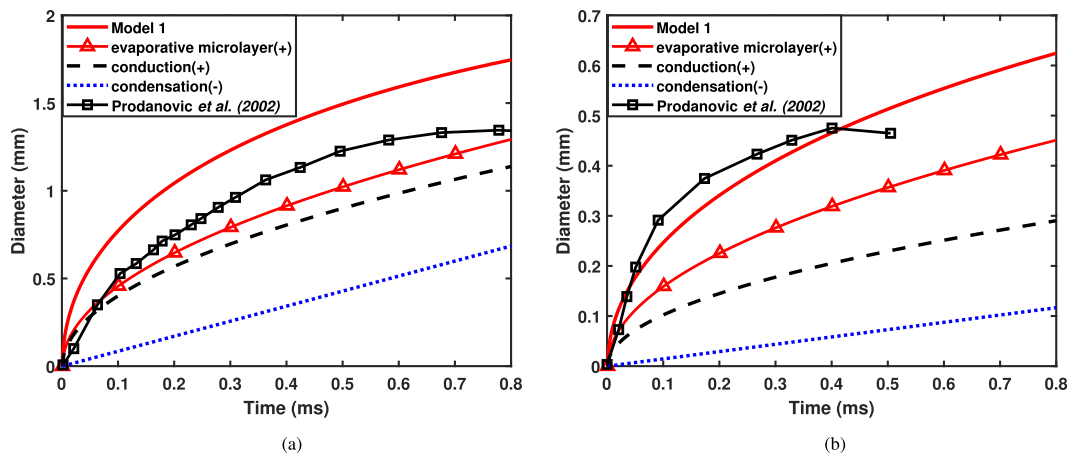


FIG. 5. Bubble diameter contribution corresponding to various components of heat transfer for pressures (a) $p = 1$ bar and (b) $p = 3$ bar.

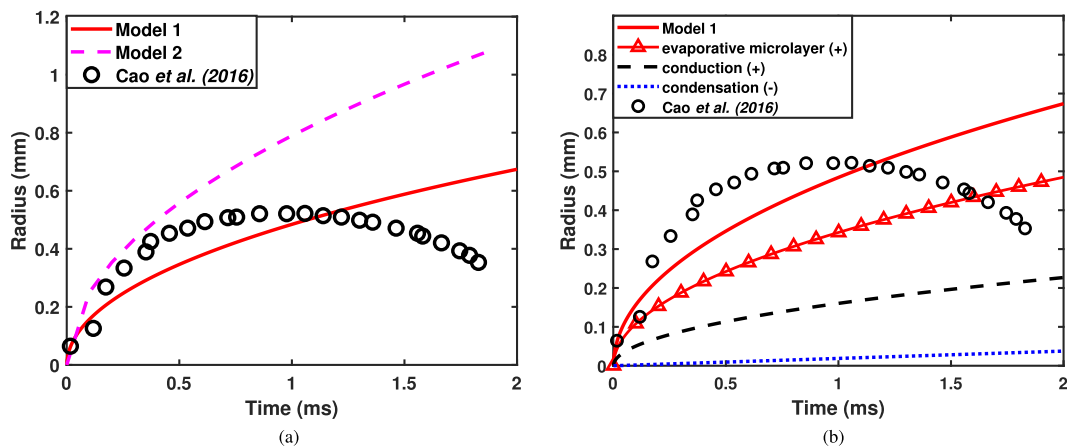


FIG. 6. (a) Comparison of the present model 1 and model 2 predictions against the experimental data of Cao *et al.*³⁷ and (b) bubble radius contribution corresponding to the individual component of heat transfer. Model 1 accounts for all three effects (microlayer evaporation, conduction, and condensation), while model 2 refers to only the conduction effect.

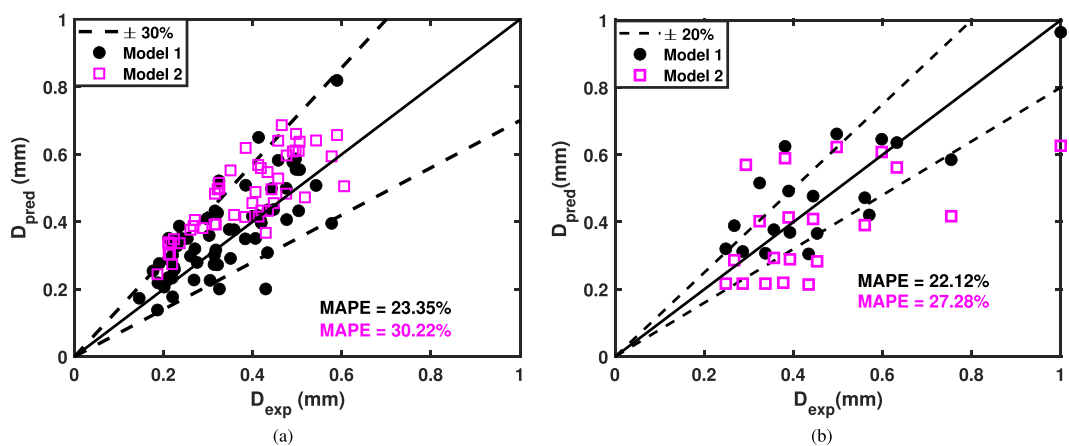


FIG. 7. Comparison of bubble departure diameter for the subcooled flow boiling conditions against the experimental data of (a) Situ *et al.*⁸ and (b) Sugrue.⁹ Model 1 accounts for all three effects (microlayer evaporation, conduction, and condensation), while model 2 refers to only the conduction effect. Mean absolute percentage error (MAPE) = $\frac{1}{N} \sum \left| \frac{D_{pred} - D_{exp}}{D_{exp}} \right| \times 100$.

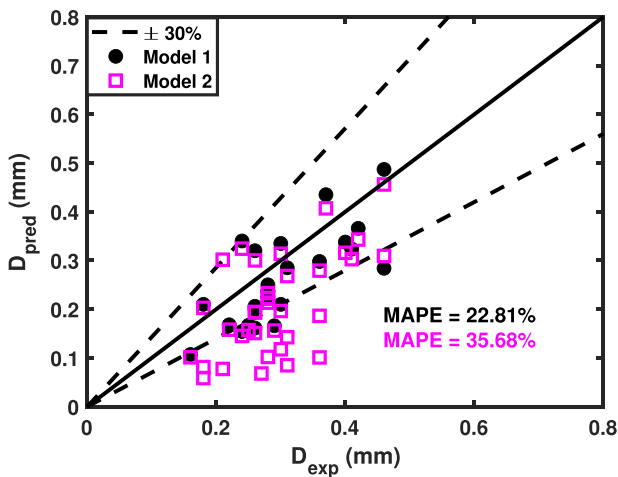


FIG. 8. Comparison of bubble departure diameter against the experimental data of Klausner *et al.*⁷ Mean absolute percentage error (MAPE) = $\frac{1}{N} \sum \left| \frac{D_{pred} - D_{exp}}{D_{exp}} \right| \times 100$.

sign as indicated in the legend. A similar behavior is also observed in Figs. 6(a) and 6(b) when model 1 and model 2 are compared with the experimental data of Cao *et al.*³⁷ for low mass flux and high subcooling conditions. A major part of the bubble growth is contributed by the microlayer evaporation.

The comparison studies shown in Figs. 4–6 represent the validation of the bubble growth model predictions. For the prediction of bubble departure diameter, force balance model is coupled with the bubble growth model for the validation against the experimental data^{7–9} for both subcooled and saturated flow boiling conditions. For the subcooled flow boiling conditions, Fig. 7 depicts comparison of bubble departure diameter against the experimental data of Situ *et al.*⁸ and Sugrue *et al.*⁹ The present model predictions are found to be in good agreement within $\pm 30\%$ deviation. The bubble departure diameter predictions for the saturated flow boiling conditions is compared

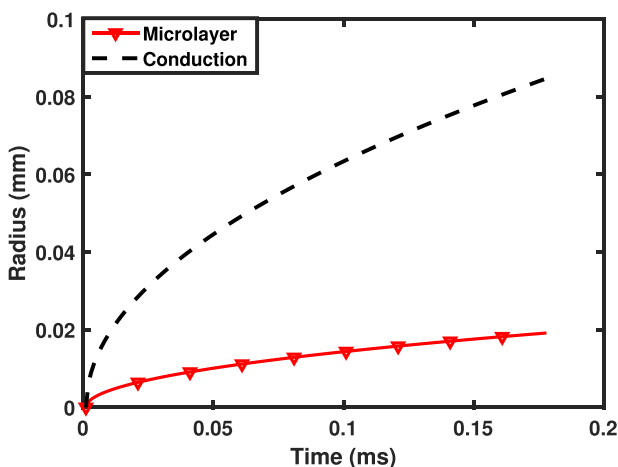


FIG. 9. Bubble diameter contribution corresponding to various components of heat transfer for the saturated flow boiling for R-113 as working fluid.

against the experimental data of Klausner *et al.*⁷ A good agreement is noticed with a $\pm 30\%$ deviation as shown in Fig. 8. Klausner *et al.*⁷ used R113 as the coolant at saturated temperature in a heated square channel. In the present study, simulations are systematically performed with and without the presence of microlayer. From the literature, the presence of microlayer for R113 is considered by Zhou *et al.*,¹⁴ Mazzocco *et al.*,⁴⁰ Raj *et al.*,¹⁶ and Colombo and Fairweather¹⁵ in their respective studies. However, Ren *et al.*⁴¹ did not consider the microlayer even though the working fluid was water. Therefore, the presence of microlayer, and the contribution of heat transfer due to the microlayer evaporation, may be proven significant or insignificant by performing numerical studies. Figure 9 presents the bubble growth rate of R113 with and without the presence of the microlayer. The contribution of the microlayer evaporation is very minimal in the case of R113, which is in line with the experimental observations. Since the present study aims at validating the bubble growth model for different sets of operating conditions against the experimental data, the presence of the microlayer is considered for the refrigerants as well. Therefore, to make the model generic for all the working fluids, the methodology of the present study is divided based on model 1 (with microlayer) and model 2 (without microlayer). Similarly, Fig. 10 shows the prediction of bubble departure diameter against the experimental data of Duhar *et al.*¹⁷

It should be noted that the bubble departs from the heated surface either by sliding or by lifting off. Although the models based on the energy and the force balance are able to accurately predict the bubble growth rate and the departure diameter, respectively, it is also important to study the bubble departure behavior. The objective of the present study is to demarcate the zones of sliding and lift-off based on the operating conditions such as, pressure, mass flux, heat flux, and subcooling. Therefore, the present study is validated against the experimental data of Situ *et al.*⁸ and Ahmadi *et al.*²⁵ for the bubble departure behavior, i.e., sliding or lifting off from the nucleation site. Situ *et al.*⁸ performed experiments to study the bubble departure diameter and its

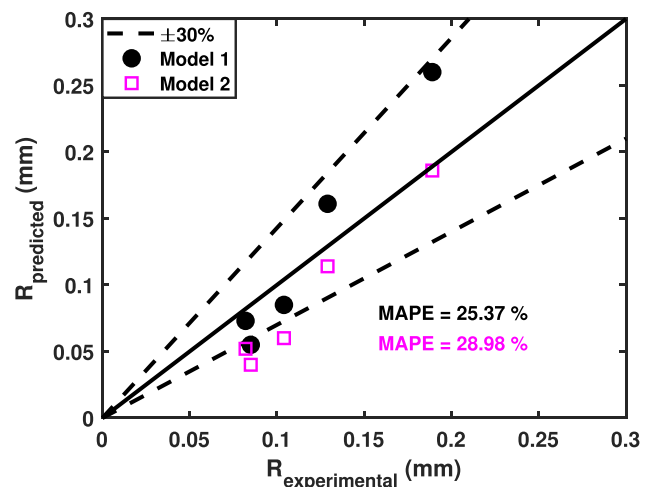


FIG. 10. Comparison of the bubble departure diameter for model 1 and model 2 against the experimental data of Duhar *et al.*¹⁷ Mean absolute percentage error (MAPE) = $\frac{1}{N} \sum \left| \frac{D_{pred} - D_{exp}}{D_{exp}} \right| \times 100$.

TABLE III. Comparison of bubble departure behavior predictions against the experimental data of Situ *et al.*⁸ Here, S and L refer to sliding and lifting-off behavior, respectively. Boiling number and absolute value of thermodynamic quality are defined as $Bo = \frac{q_w}{Gh_{fg}}$ and $|x| = \frac{c_p \Delta T_{sub}}{h_{fg}}$, respectively.

S. No.	T_{in} (°C)	Heat flux (kWm ⁻²)	Velocity (ms ⁻¹)	D_{exp} (S/L) (mm)	D_{pre} (S/L) (mm, Model 1)	D_{pre} (S/L) (mm, Model 2)	Ja	$Bo/ x $ ($\times 10^3$)
1	90	145	0.927	0.577(L)	0.3949(L)	0.5937(L)	26.175	5.565
2	90	148	0.925	0.503(L)	0.4322(L)	0.6101(L)	26.895	5.75
3	90	136	0.924	0.433(L)	0.308(L)	0.5471(L)	24.12	5.104
4	90	145	0.921	0.476(L)	0.406(L)	0.596(L)	26.289	5.61
5	90	154	0.924	0.542(L)	0.5074(L)	0.6408(L)	28.24	6.105
6	90	158	0.924	0.497(L)	0.555(L)	0.6604(L)	29.115	6.342
7	91.2	146	0.922	0.505(L)	0.554(L)	0.6372(L)	28.09	6.85
8	89	143	0.927	0.35(L)	0.291(L)	0.552(L)	24.348	4.789
9	87.6	142	0.929	0.325(L)	0.2(L)	0.499(L)	22.005	4.024
10	90	143	0.926	0.347(L)	0.377(L)	0.5846(L)	25.77	5.484
11	91.2	142	0.92	0.384(L)	0.508(L)	0.6187(L)	27.274	6.62
12	94	101	0.912	0.406(L)	0.3503(L)	0.488(L)	21.546	7.165
13	85	104	0.487	0.321(L)	0.521(L)	0.515(L)	20.7289	4.89
14	92.6	63.1	0.504	0.236(L)	0.346(L)	0.336(L)	14.826	5.15
15	91.6	62.3	0.503	0.214(L)	0.287(L)	0.0.302(L)	13.318	4.36
16	93	61.5	0.504	0.211(L)	0.351(L)	0.334(L)	14.765	5.322
17	92	61.1	0.501	0.211(L)	0.29(L)	0.304(L)	13.4378	4.522
18	91	61.5	0.507	0.219(L)	0.233(L)	0.274(L)	12.084	3.907
19	90	61.9	0.508	0.186(L)	0.138(L)	0.244(L)	10.778	3.475
20	88	99.8	0.506	0.475(L)	0.499(L)	0.483(L)	20.335	5.002
21	87	101	0.508	0.447(L)	0.436(L)	0.455(L)	19.576	4.581
22	86	101	0.507	0.358(L)	0.376(L)	0.42(L)	18.55	4.201
23	85	101	0.511	0.317(L)	0.316(L)	0.392(L)	17.318	3.835
24	84	107	0.513	0.27(L)	0.319(L)	0.405(L)	17.863	3.787
25	83	101	0.511	0.21(L)	0.234(L)	0.339(L)	14.956	3.315
26	88	95	0.506	0.434(L)	0.435(L)	0.432(L)	19.0801	4.725
27	87	106	0.51	0.442(L)	0.498(L)	0.496(L)	20.8762	4.852
28	86	105	0.51	0.399(L)	0.416(L)	0.455(L)	19.594	4.383
29	85	98.2	0.509	0.26(L)	0.298(L)	0.376(L)	16.5944	3.737
30	88	105	0.504	0.457(L)	0.582(L)	0.528(L)	21.738	5.363

behavior in an annular test section for near atmospheric pressure conditions, wherein the inner rod in the annulus is heated. They reported that, the bubble departs by lifting off from the heated surface for the considered operating conditions, $Ja < 30$. Table III presents the predicted bubble departure diameter and behavior using model 1 and model 2. Both the models predicted the bubble lift-off behavior in line with the experimental observations. However, model 1 (MAPE = 23.35%) predictions of bubble departure diameter are better compared to that of the model 2 (MAPE = 30.22%), as shown in Fig. 7(a).

Ahmadi *et al.*²⁵ have conducted experiments to study the bubble departure behavior in a rectangular channel using a high speed camera. Figure 11 shows the comparison of the present models against the experimental data of Ahmadi *et al.*²⁵ A good agreement is noticed with a mean percentage error of around 25% and 28% for model 1 and model 2, respectively. Furthermore, Ahmadi *et al.*²⁵ have observed

that the sliding and lifting-off behavior of the vapor bubble is dependent on Jakob number ($Ja = \frac{\rho_l c_p (T_w - T_{sat})}{\rho_g h_{fg}}$), which is an indicator of operating pressure. They have essentially classified bubble behavior based on Jakob number (Ja). For $Ja > 35$, the bubble lift-off from the heated surface was observed, whereas sliding behavior along the heated surface was noticed for $Ja < 35$. However, the influence of mass flux, heat flux, and subcooling is not directly accounted for. Therefore, instead of Ja , the combination of boiling number ($Bo = \frac{q_w}{Gh_{fg}}$) and thermodynamic quality ($|x| = \frac{c_p \Delta T_{sub}}{h_{fg}}$) i.e., $Bo/|x| = \frac{q_w}{Gc_p \Delta T_{sub}}$ is used in the present study for describing the departure behavior of bubbles. Table IV presents the comparison of bubble departure diameter and behavior against the experimental data of Ahmadi *et al.*²⁵ Based on $Bo/|x|$ (Table IV) values, if $Bo/|x| > 11.3 \times 10^{-3}$ and $Ja > 35$, the bubble lifts off, whereas the bubble departs by

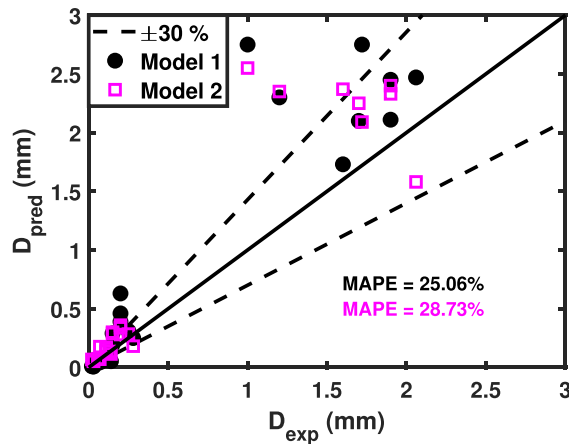


FIG. 11. Comparison of the bubble departure diameter for model 1 and model 2 against the experimental data of Ahmadi *et al.*²⁵ Mean absolute percentage error (MAPE) = $\frac{1}{N} \sum \left| \frac{D_{pred} - D_{exp}}{D_{exp}} \right| \times 100$.

TABLE IV. Comparison of bubble departure behavior predictions against the experimental data of Ahmadi *et al.*²⁵ Here, S and L refer to sliding and lifting-off behavior, respectively. Boiling number and absolute value of thermodynamic quality are defined as $Bo = \frac{q_w}{G h_{fg}}$ and $|x| = \frac{c_p \Delta T_{sub}}{h_{fg}}$, respectively.

S. No.	Pressure (kPa)	Mass flux ($\text{kgm}^{-2}\text{s}^{-1}$)	Heat flux (kWm^{-2})	D_{exp} (S/L) (mm)	D_{pre} (S/L) (mm, Model 1)	D_{pre} (S/L) (mm, Model 2)	Ja	$Bo/ x $ ($\times 10^3$)
1	100	169	160	1.70(L)	2.10(S)	2.25(S)	38.15	28.73
2	100	169	170	3.9(L)	1.93(S)	2.30(S)	38.74	22.39
3	100	170	189	1.60(L)	1.73(S)	2.37(S)	39.65	15.83
4	98	260	200	1.90(L)	2.11(S)	2.40(S)	40.25	14.381
5	100	325	200	1.90(L)	2.45(S)	2.23(L)	40.04	14.127
6	100	325	220	1.20(L)	2.3(S)	2.35(L)	41.24	11.90
7	98	392	166	2.06(L)	2.47(S)	1.58(L)	36.10	14.54
8	97	384	224	1.72(L)	2.75(S)	2.09(L)	42.02	12.988
9	101	388	289	1.00(L)	2.75(S)	2.55(L)	47.24	11.302
10	198	325	132	0.25(S)	0.31(S)	0.28(L)	10.85	11.04
11	201	386	213	0.20(S)	0.46(L)	0.36(L)	14.75	10.61
12	201	386	229	0.20(S)	0.29(L)	0.36(L)	12.64	9.45
13	192	785	230	0.15(S)	0.19(L)	0.30(L)	13.28	6.13
14	406	762	123	0.14(S)	0.062(S)	0.11(S)	5.51	9.82
15	404	768	158	0.13(S)	0.078(S)	0.136(S)	6.37	8.604
16	407	764	207	0.11(S)	0.091(S)	0.138(S)	7.26	7.13
17	405	761	272	0.11(S)	0.115(S)	0.159(S)	8.58	6.86
18	403	761	328	0.11(S)	0.123(S)	0.173(S)	9.40	6.329
19	406	1170	301	0.07(S)	0.032(S)	0.14(S)	7.51	4.547
20	400	1170	357	0.07(S)	0.0452(S)	0.15(S)	8.53	4.55
21	397	1170	442	0.07(S)	0.063(S)	0.177(S)	9.92	4.549
22	802	377	172	0.06(S)	0.056(S)	0.074(S)	3.06	10.031
23	799	380	213	0.06(S)	0.06(S)	0.074(S)	3.48	9.986
24	808	384	252	0.06(S)	0.059(S)	0.071(S)	3.74	8.92
25	809	1091	198	0.03(S)	0.0087(S)	0.052(S)	2.64	5.15
26	806	1100	275	0.03(S)	0.01(S)	0.058(S)	3.25	4.785
27	797	1094	345	0.02(S)	0.013(S)	0.068(S)	3.86	4.81
28	798	1122	414	0.02(S)	0.015(S)	0.054(S)	4.33	4.69

sliding along the heated surface if $Bo/|x| < 11.3 \times 10^{-3}$ and $Ja < 35$. However, the experimental data of Situ *et al.*⁸ report a lift-off behavior for $Ja < 30$ and $Bo/|x| < 7.2 \times 10^{-3}$ (Table III). The values of Ja and $Bo/|x|$ for the Ahmadi *et al.*²⁵ and Situ *et al.*⁸ are very close to each other. From the validation studies discussed in the present study (Sec. III A), it can be inferred that (i) both the models are validated against the experimental data for bubble growth rate, bubble departure diameter, and behavior, and (ii) model 1 has better predictions compared to model 2. However, it should be noted that the bubble departure behavior predictions by both the models are not so different. Therefore, model 1 is preferred for further calculations to investigate the effect of the operating conditions on bubble growth rate and departure.

B. Influence of operating parameters

In the present study, the flow boiling through a heated vertical annular channel is investigated. The heated inner rod has a diameter of 19 mm, and the annular section is of 38 mm diameter, with an effective hydraulic diameter of 19 mm, also, the advancing and receding contact angles used are $\pi/4$ and $\pi/5$, respectively.⁸ When the

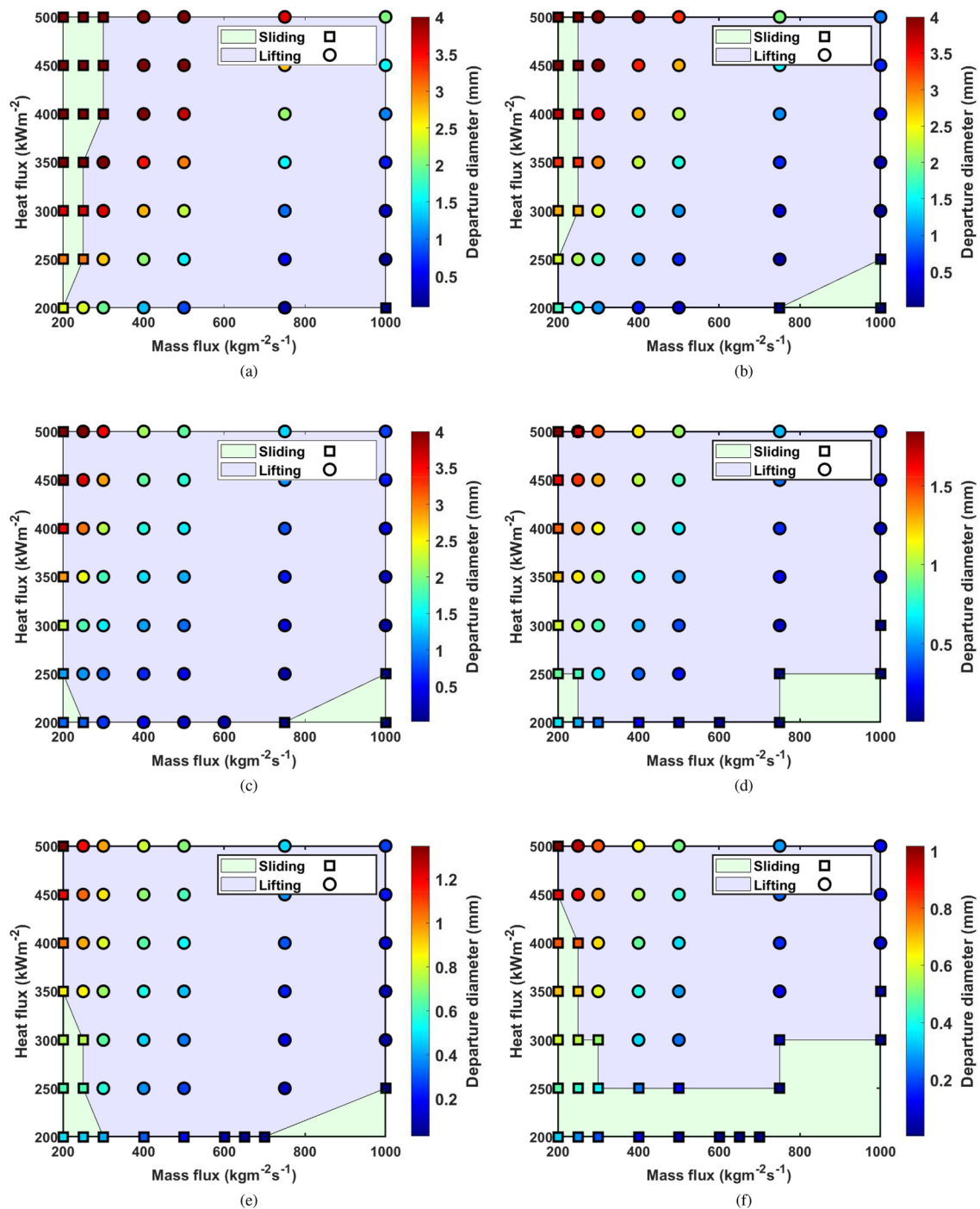


FIG. 12. Identification of the region of sliding and lift-off for the bubble from the heated surface for pressure varying from 1 to 3 bar and subcooling of $\Delta T_{\text{sub}} = 20\text{--}30\text{ }^{\circ}\text{C}$.

temperature of the heated surface is sufficiently greater than the saturation temperature of the liquid, bubble nucleation is initiated. The bubble continues to grow as it extracts heat from the surface and eventually departs after reaching its critical size. The bubble departure

from the heated surface is of two types: (a) bubble slides along the heated surface (if $\sum F_x > 0$) and (b) lifts off from the heated surface (if $\sum F_y > 0$). Bubble departure diameter is calculated using force balance approach, while some bubbles slide and some lift off from the

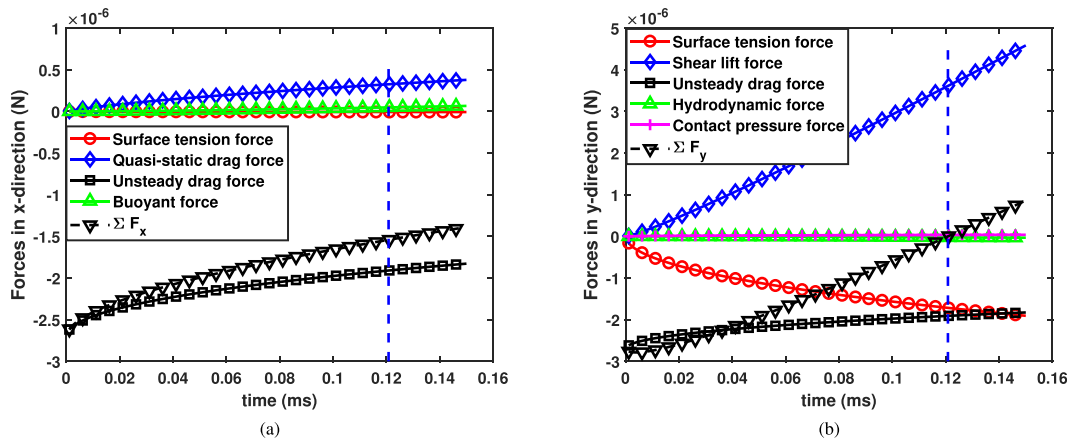


FIG. 13. Forces in (a) x-direction and (b) y-direction for $p = 1$ bar, $G = 750 \text{ kgm}^{-2}\text{s}^{-1}$, and for the subcooling of $\Delta T_{\text{sub}} = 20^\circ\text{C}$.

heated surface. In order to demarcate the region of sliding and lift-off behavior, the following operating conditions were chosen: pressure (p) = 1–3 bar, mass flux (G) = 200–1000 $\text{kgm}^{-2}\text{s}^{-1}$, heat flux (q_w) = 200–500 kWm^{-2} , and degree of subcooling (ΔT_{sub}) = 20 and 30°C .

For a given pressure and subcooling conditions, the mass flux was varied from 200–1000 $\text{kgm}^{-2}\text{s}^{-1}$ and the heat flux was varied from 200–500 kWm^{-2} . The operating parametric space was covered for the entire range of pressure, mass flux, subcooling, and heat flux, to determine whether the bubble slides or lifts off from the heated surface. Following Lee *et al.*,⁴² the maximum bubble departure diameter is restricted to 4 mm. Based on detailed simulations over the parametric space, the regime map for the bubble behavior is generated in Fig. 12. Figures 12(a), 12(c), and 12(e) refer to subcooling of $\Delta T_{\text{sub}} = 20^\circ\text{C}$, whereas Figs. 12(b), 12(d), and 12(f) is for the subcooling of $\Delta T_{\text{sub}} = 30^\circ\text{C}$. Figures 12(a) and 12(b) is for the pressure of 1 bar, Figs. 12(c) and 12(d) is for the pressure of 2 bars and Figs. 12(e) and 12(f) refers to the pressure of 3 bars. It can be noticed from Figs. 12(a) and 12(b) that as the degree of subcooling increases from 20 to 30°C the sliding zone contracts for a pressure of 1 bar and mass flux

($G < 250 \text{ kgm}^{-2}\text{s}^{-1}$). However, with increase in mass flux ($G \geq 750 \text{ kgm}^{-2}\text{s}^{-1}$) for low heat flux ($q_w \leq 250 \text{ kWm}^{-2}$), there is an increase in the zone of sliding. Furthermore, for higher pressures (2 and 3 bar), with low mass flux ($G < 250 \text{ kgm}^{-2}\text{s}^{-1}$) and high heat flux ($q_w \geq 350 \text{ kWm}^{-2}$), there is further contraction in the sliding zone. With increase in mass flux and degree of subcooling for higher pressure, there is an increase in the sliding zone. In Fig. 12, there is variation in the pattern of sliding and lift-off zones, which can be explained by analyzing individual contribution of forces as shown in Figs. 13 and 14.

In the sliding zone, the sum of the quasi-static drag force [Eq. (23)] and the force of buoyancy [Eq. (24)] are more significant as compared to other forces acting along the heated surface (in the x-direction). On the contrary, in the y-direction, the unsteady drag force [Eq. (22)] dominates the forces that oppose the bubble detachment by lift-off. As a result, the resultant force acts along the positive x-direction (as $\sum F_x > 0$), and hence, the bubble departs by sliding along the heated surface. Whereas, in the lift-off zone, the normal force equilibrium gets disturbed ($\sum F_y > 0$) for the bubble to lift off. It is commonly observed that, in the lift-off zone, shear lift force is dominant,

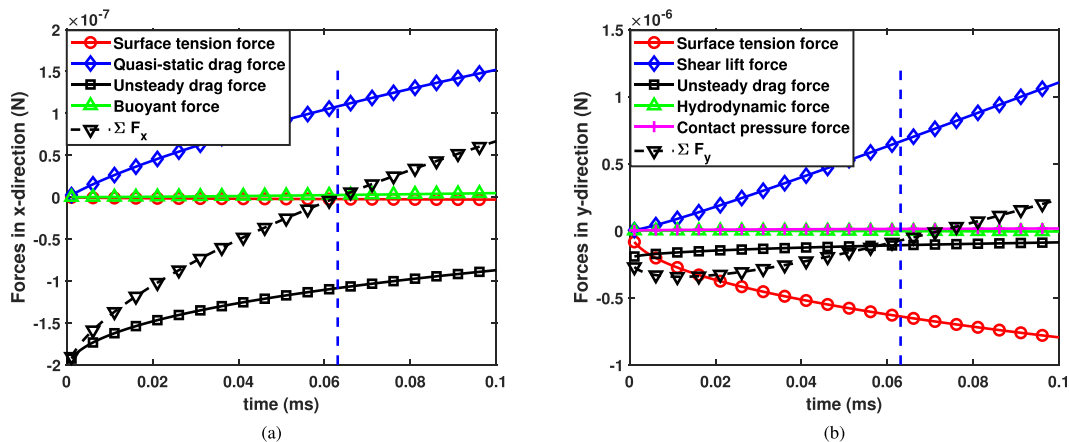


FIG. 14. Forces in (a) x-direction and (b) y-direction for $p = 1$ bar, $G = 1000 \text{ kgm}^{-2}\text{s}^{-1}$, and for the subcooling of $\Delta T_{\text{sub}} = 20^\circ\text{C}$.

TABLE V. Variation of $Bo/|x|$ for sliding and lifting-off behavior of the bubble. Boiling number (Bo) and thermodynamic quality (x) are defined as $Bo = \frac{q_w}{Gh_{fg}}$ and $|x| = \frac{c_p \Delta T_{sub}}{h_{fg}}$, respectively.

S. No.	Pressure (bar)	Heat flux (kWm^{-2})	Lifting		Sliding	
1	1	$q_w \leq 250$	$3 < \left(\frac{Bo}{ x }\right) \times 10^3 < 8$	$20 < Ja < 40$	$\left(\frac{Bo}{ x }\right) \times 10^3 > 8$ or $\left(\frac{Bo}{ x }\right) \times 10^3 < 3$	$Ja > 40$ or $Ja < 20$
		$300 \leq q_w \leq 350$	$\left(\frac{Bo}{ x }\right) \times 10^3 < 10$	$Ja < 50$	$\left(\frac{Bo}{ x }\right) \times 10^3 > 10$	$Ja > 50$
		$400 \leq q_w \leq 500$	$\left(\frac{Bo}{ x }\right) \times 10^3 < 14$	$Ja < 60$	$\left(\frac{Bo}{ x }\right) \times 10^3 > 14$	$Ja > 60$
2	2	$q_w \leq 250$	$4 < \left(\frac{Bo}{ x }\right) \times 10^3 < 6$	$7 < Ja < 17$	$\left(\frac{Bo}{ x }\right) \times 10^3 > 6$ or $\left(\frac{Bo}{ x }\right) \times 10^3 < 4$	$Ja > 17$ or $Ja < 7$
		$300 \leq q_w \leq 350$	$3 < \left(\frac{Bo}{ x }\right) \times 10^3 < 14$	$13 < Ja < 24$	$\left(\frac{Bo}{ x }\right) \times 10^3 > 14$ or $\left(\frac{Bo}{ x }\right) \times 10^3 < 3$	$Ja > 24$ or $Ja < 13$
		$400 \leq q_w \leq 500$	$\left(\frac{Bo}{ x }\right) \times 10^3 < 16$	$Ja < 30$	$\left(\frac{Bo}{ x }\right) \times 10^3 > 16$	$Ja > 30$
3	3	$q_w \leq 250$	$6 < \left(\frac{Bo}{ x }\right) \times 10^3 < 7$	$4 < Ja < 10$	$\left(\frac{Bo}{ x }\right) \times 10^3 > 7$ or $\left(\frac{Bo}{ x }\right) \times 10^3 < 6$	$Ja > 10$ or $Ja < 4$
		$300 < q_w < 350$	$2.5 < \left(\frac{Bo}{ x }\right) \times 10^3 < 10$	$Ja < 14$	$\left(\frac{Bo}{ x }\right) \times 10^3 > 10$ or $\left(\frac{Bo}{ x }\right) \times 10^3 < 2.5$	$Ja > 14$
		$400 < q_w < 500$	$\left(\frac{Bo}{ x }\right) \times 10^3 < 17$	$Ja < 20$	$\left(\frac{Bo}{ x }\right) \times 10^3 > 17$	$Ja > 20$

compared to the other components along the normal direction. This is further corroborated by the fact that the dominance of unsteady drag and surface tension forces is responsible for impeding the bubble from sliding. As the subcooling increases, more heat is transferred to the subcooled region, which results in an increase in the portion of the bubble that is exposed to the bulk subcooled liquid. This further recedes the bubble growth due to which the bubble departure diameter decreases. As a consequence, the force of buoyancy decreases much faster compared to the unsteady drag force. Hence, the combined effect of the quasi-static drag force and buoyant force becomes less

than the unsteady drag force. For low mass flux conditions, due to the decrease in unsteady drag force, the shear lift force starts dominating and the bubble lift off from the heated surface.

For higher mass flux conditions (Fig. 12), bubble sliding is noticed for low heat flux. With increase in mass flux (for low heat flux condition), with an attendant decrease in Ja , bubble departure diameter decreases. Due to this, the unsteady drag force decreases; hence, in the x -direction, the sum of quasi-static drag force and buoyant force dominates these opposing forces. However, in the y -direction, the detaching forces on the bubble are not able to overcome the attaching

forces. Hence, the bubble starts sliding for high mass flux and low heat flux conditions.

Similarly, with increase in pressure, for higher heat flux, the sliding zone contracts. On the contrary, the sliding zone expands for low heat flux conditions. Thus, with increase in pressure, the bubble diameter decreases. This is due to a faster rate of decrease in buoyancy force (varies as cube of bubble radius) compared to the unsteady drag force (varies as square of radius). This results in the domination of the unsteady drag force in the x -direction, hindering the bubble from the sliding behavior. Hence, the bubble lifts off from the heated surface. For low heat flux and low mass flux conditions, the sliding zone expands. For low heat flux, Ja decreases, causing the bubble diameter to decrease further. This would effectively decrease the unsteady drag force and buoyant force in the x -direction, and the bubble starts sliding. In Figs. 13 and 14, the vertical dotted line refers to the time of the bubble departure. Associated force balances at the point of departure are particularly noteworthy. Table V summarizes the sliding and lifting behavior of the bubble in terms of boiling number (Bo) and thermodynamic quality ($|x|$). Under the influence of pressure, the non-dimensional quantity is distinguished based on low heat flux ($q_w \leq 250 \text{ kWm}^{-2}$), moderate heat flux ($300 \leq q_w \leq 350 \text{ kWm}^{-2}$), and high heat flux ($400 \leq q_w \leq 500 \text{ kWm}^{-2}$).

IV. CONCLUSIONS

In the present study, a numerical model based on energy balance and force balance was developed for the prediction of bubble growth rate and the departure diameter. The bubble departure behavior is predicted based on the resultant unbalanced (positive) force on the bubble in either the direction along the heated surface ($\Sigma F_x > 0$) for sliding or normal to the heated surface ($\Sigma F_y > 0$) for lift-off. Validation studies were carried out against the available experimental data for the flow boiling conditions. Furthermore, numerical studies were extended to predict the bubble growth rate, departure diameter, and behavior by varying the operating conditions such as pressure (1–3 bar), inlet mass flux ($200\text{--}1000 \text{ kgm}^{-2}\text{s}^{-1}$), wall heat flux ($200\text{--}500 \text{ kWm}^{-2}$), and subcooling ($\Delta T_{\text{sub}} = 20\text{--}30^\circ\text{C}$). In the present study, it is observed that (i) the size of the bubble increases with an increase in heat flux (for constant mass flux and subcooling), (ii) bubble departure diameter decreases with increase in pressure, while keeping other parameters unchanged, and (iii) bubble departs by sliding over the heated surface for low mass flux ($200\text{--}250 \text{ kgm}^{-2}\text{s}^{-1}$). As the subcooling increases ($\Delta T_{\text{sub}} = 30^\circ\text{C}$) for constant pressure, the sliding zone was found to contract. At high mass flux conditions ($G > 750 \text{ kgm}^{-2}\text{s}^{-1}$), it is noticed that the bubble lifts off from the nucleation site, but for low heat flux conditions ($q \leq 250 \text{ kWm}^{-2}$), the bubble departs by sliding along the heated surface. Demarcation of zones of sliding and lifting off of the bubble is expressed in terms of ($Bo/|x|$). Based on the force balance approach, the sliding behavior of the bubble is observed when buoyancy force and quasi-static drag forces are dominant in the flow direction. However, for the lift-off behavior, i.e., bubble departure in the direction normal to the heated surface is dominated by shear lift force over surface tension and unsteady drag force. As the mass flux increases, shear lift force increases and the bubble lifts off. However, for high mass flux ($G > 750 \text{ kgm}^{-2}\text{s}^{-1}$), the inertial force of the flow increases and the bubble departs by sliding.

AUTHOR DECLARATIONS

Conflict of Interest

The authors have no conflicts to disclose.

Author Contributions

Nikhil Chitnavis: Data curation (equal); Formal analysis (equal); Investigation (equal); Methodology (equal); Software (equal); Validation (equal); Visualization (equal); Writing – original draft (equal). **Harish Pothukuchi:** Conceptualization (equal); Data curation (equal); Formal analysis (equal); Funding acquisition (equal); Methodology (equal); Project administration (equal); Supervision (equal); Validation (equal); Writing – review & editing (equal). **B. S. V. Patnaik:** Conceptualization (equal); Funding acquisition (equal); Methodology (equal); Project administration (equal); Resources (equal); Supervision (equal); Writing – review & editing (equal).

DATA AVAILABILITY

The data that support the findings of this study are available from the corresponding author upon reasonable request.

NOMENCLATURE

Bo	Boiling number $[\frac{q_w}{Gh_{fg}}]$
C_p	Specific heat ($\text{kJ/kg} - \text{K}$)
D_h	Hydraulic diameter (m)
d_b	Bubble departure diameter (mm)
d_w	Contact diameter (mm)
f	Portion of bubble in contact of subcooled liquid
G	Mass flux ($\text{kgm}^{-2}\text{s}^{-1}$)
g	Gravitational acceleration (m/s^2)
h	Convective heat transfer coefficient ($\text{Wm}^{-2}\text{s}^{-1}$)
h_{lv}	Latent heat (kJkg^{-1})
Ja	Jakob number $[\frac{\rho_l C_{pl} (T_w - T_{\text{sat}})}{\rho_s h_{fg}}]$
k	Thermal diffusivity ($\text{Wm}^{-1}\text{K}^{-1}$)
q_w	Wall heat flux (kWm^{-2})
Re	Reynolds number
R_b	Bubble radius (mm)
S	Suppression factor
T	Temperature (K)
T_τ	Frictional temperature (K)
t	Time (s)
u_*	Frictional velocity (m/s)
$ x $	Thermodynamic quality $[\frac{C_p (T_{\text{sat}} - T_{\text{bulk}})}{h_{fg}}]$
y	Wall distance (m)
y^+	Non-dimensional wall distance
α	Thermal diffusivity (m^2/s)

Greek letters

α	Advancing contact angle
β	Receding contact angle
ϕ	Inclination of bubble
θ	Inclination of heated surface
ρ	Density of fluid (kgm^{-3})
μ	Dynamic viscosity of fluid ($\text{kgm}^{-1}\text{s}^{-1}$)

σ Surface tension (N/m)
 τ Shear stress/friction

Subscripts

cond Condensation
 conv Convection
 d Departure
 nb Nucleate boiling
 sat Saturation
 sub Subcooling
 w Wall

REFERENCES

- ¹P. Kangude and A. Srivastava, "On the mechanisms leading to ordered nano-particles deposition during single bubble nucleate pool boiling regime," *Phys. Fluids* **33**, 113306 (2021).
- ²S. Saisorn, A. Suriyawong, P. Srithumkhan, P. Wongpromma, and S. Wongwiset, "An investigation of horizontal and vertical flow boiling in a single channel with a confinement number beyond the threshold of micro-scale flow," *Phys. Fluids* **33**, 113302 (2021).
- ³M. Moiz, S. R. G. Vadlamudi, and A. Srivastava, "Experiments to understand microlayer and dry patch dynamics under subcooled nucleate flow boiling in a vertically-oriented rectangular channel," *Phys. Fluids* **35**, 043320 (2023).
- ⁴J. Broughton and Y. K. Joshi, "Flow boiling in geometrically modified micro-channels," *Phys. Fluids* **33**, 103308 (2021).
- ⁵L. Fei, J. Yang, Y. Chen, H. Mo, and K. H. Luo, "Mesoscopic simulation of three-dimensional pool boiling based on a phase-change cascaded lattice Boltzmann method," *Phys. Fluids* **32**, 103312 (2020).
- ⁶L. Fei, F. Qin, J. Zhao, D. Derome, and J. Carmeliet, "Lattice Boltzmann modelling of isothermal two-component evaporation in porous media," *J. Fluid Mech.* **955**, A18 (2023).
- ⁷J. F. Klausner, R. Mei, D. Bernhard, and L. Zeng, "Vapor bubble departure in forced convection boiling," *Int. J. Heat Mass Transfer* **36**, 651–662 (1993).
- ⁸R. Situ, T. Hibiki, M. Ishii, and M. Mori, "Bubble lift-off size in forced convective subcooled boiling flow," *Int. J. Heat Mass Transfer* **48**, 5536–5548 (2005).
- ⁹R. Sugrue, J. Buongiorno, and T. McKrell, "An experimental study of bubble departure diameter in subcooled flow boiling including the effects of orientation angle, subcooling, mass flux, heat flux, and pressure," *Nucl. Eng. Des.* **279**, 182–188 (2014).
- ¹⁰M. Bucci, J. Buongiorno, and M. Bucci, "The not-so-subtle flaws of the force balance approach to predict the departure of bubbles in boiling heat transfer," *Phys. Fluids* **33**, 017110 (2021).
- ¹¹J. Du, C. Zhao, and H. Bo, "Investigation of bubble departure diameter in horizontal and vertical subcooled flow boiling," *Int. J. Heat Mass Transfer* **127**, 796–805 (2018).
- ¹²N. Zuber, "The dynamics of vapor bubbles in nonuniform temperature fields," *Int. J. Heat Mass Transfer* **2**, 83–98 (1961).
- ¹³N. Kurul and M. Z. Podowski, "Multidimensional effects in forced convection subcooled boiling," in *International Heat Transfer Conference Digital Library* (Begel House, Inc., 1990).
- ¹⁴P. Zhou, R. Huang, S. Huang, Y. Zhang, and X. Rao, "Experimental investigation on bubble contact diameter and bubble departure diameter in horizontal subcooled flow boiling," *Int. J. Heat Mass Transfer* **149**, 119105 (2020).
- ¹⁵M. Colombo and M. Fairweather, "Prediction of bubble departure in forced convection boiling: A mechanistic model," *Int. J. Heat Mass Transfer* **85**, 135–146 (2015).
- ¹⁶S. Raj, M. Pathak, and M. K. Khan, "An analytical model for predicting growth rate and departure diameter of a bubble in subcooled flow boiling," *Int. J. Heat Mass Transfer* **109**, 470–481 (2017).
- ¹⁷G. Duhar, G. Riboux, and C. Colin, "Vapour bubble growth and detachment at the wall of shear flow," *Heat Mass Transfer* **45**, 847–855 (2009).
- ¹⁸J. Yoo, C. E. Estrada-Perez, and Y. A. Hassan, "Development of a mechanistic model for sliding bubbles growth prediction in subcooled boiling flow," *Appl. Therm. Eng.* **138**, 657–667 (2018).
- ¹⁹J. Yoo, C. E. Estrada-Perez, and Y. A. Hassan, "Experimental study on bubble dynamics and wall heat transfer arising from a single nucleation site at sub-cooled flow boiling conditions—Part 2: Data analysis on sliding bubble characteristics and associated wall heat transfer," *Int. J. Multiphase Flow* **84**, 292–314 (2016).
- ²⁰H. Ünal, "Maximum bubble diameter, maximum bubble-growth time and bubble-growth rate during the subcooled nucleate flow boiling of water up to 17.7 MN/m²," *Int. J. Heat Mass Transfer* **19**, 643–649 (1976).
- ²¹D. Legendre, C. Colin, and T. Coquard, "Lift, drag and added mass of a hemispherical bubble sliding and growing on a wall in a viscous linear shear flow," *Philos. Trans. R. Soc. A* **366**, 2233–2248 (2008).
- ²²C. van der Geld, "The dynamics of a boiling bubble before and after detachment," *Heat Mass Transfer* **45**, 831–846 (2009).
- ²³S. Zanje, K. Iyer, J. S. Murallidharan, H. Puneekar, and V. K. Gupta, "Development of generalized bubble growth model for cavitation and flash boiling," *Phys. Fluids* **33**, 077116 (2021).
- ²⁴I. W. Park, I. Y. Kang, J. Yu, and Y.-G. Lee, "Bubble lift-off diameter of lifting-off and ejecting bubbles in subcooled flow boiling," *Int. Commun. Heat Mass Transfer* **129**, 105727 (2021).
- ²⁵R. Ahmadi, T. Ueno, and T. Okawa, "Bubble dynamics at boiling incipience in subcooled upward flow boiling," *Int. J. Heat Mass Transfer* **55**, 488–497 (2012).
- ²⁶M. Cooper and A. Lloyd, "The microlayer in nucleate pool boiling," *Int. J. Heat Mass Transfer* **12**, 895–913 (1969).
- ²⁷W. Ranz and W. Marshal, "Evaporation from drops, parts I & II," *Chem. Eng. Prog.* **48**, 141–146 (1952).
- ²⁸J. C. Chen, "Correlation for boiling heat transfer to saturated fluids in convective flow," *Ind. Eng. Chem. Process Des. Dev.* **5**, 322–329 (1966).
- ²⁹K. E. Gungor and R. Winterton, "A general correlation for flow boiling in tubes and annuli," *Int. J. Heat Mass Transfer* **29**, 351–358 (1986).
- ³⁰B. Kader, "Temperature and concentration profiles in fully turbulent boundary layers," *Int. J. Heat Mass Transfer* **24**, 1541–1544 (1981).
- ³¹B.-J. Yun, A. Splawski, S. Lo, and C.-H. Song, "Prediction of a subcooled boiling flow with advanced two-phase flow models," *Nucl. Eng. Des.* **253**, 351–359 (2012).
- ³²R. Mei and J. Klausner, "Shear lift force on spherical bubbles," *Int. J. Heat Fluid Flow* **15**, 62–65 (1994).
- ³³T. Auton, "The lift force on a spherical body in a rotational flow," *J. Fluid Mech.* **183**, 199–218 (1987).
- ³⁴S. R. G. Vadlamudi, G. K. Sinha, A. Srivastava, and S. Singh, "Dynamic interaction of growing bubble and microlayer: Need for reconciliation of experiments and theory in flow boiling," *Appl. Phys. Lett.* **121**, 124101 (2022).
- ³⁵R. Mei and J. F. Klausner, "Unsteady force on a spherical bubble at finite Reynolds number with small fluctuations in the free-stream velocity," *Phys. Fluids A* **4**, 63–70 (1992).
- ³⁶V. Prodanovic, D. Fraser, and M. Salcudean, "Bubble behavior in subcooled flow boiling of water at low pressures and low flow rates," *Int. J. Multiphase Flow* **28**, 1–19 (2002).
- ³⁷Y. Cao, Z. Kawara, T. Yokomine, and T. Kunugi, "Visualization study on bubble dynamical behavior in subcooled flow boiling under various subcooling degree and flowrates," *Int. J. Heat Mass Transfer* **93**, 839–852 (2016).
- ³⁸MATLAB, Version 7.10.0 (R2021a) (The MathWorks, Inc., Natick, MA, 2021).
- ³⁹B. Mikic, W. Rohsenow, and P. Griffith, "On bubble growth rates," *Int. J. Heat Mass Transfer* **13**, 657–666 (1970).
- ⁴⁰T. Mazzocco, W. Ambrosini, R. Kommajosyula, and E. Baglietto, "A reassessed model for mechanistic prediction of bubble departure and lift off diameters," *Int. J. Heat Mass Transfer* **117**, 119–124 (2018).
- ⁴¹T. Ren, Z. Zhu, R. Zhang, J. Shi, and C. Yan, "Development of force balance model for prediction of bubble departure diameter and lift-off diameter in subcooled flow boiling," *Int. J. Heat Mass Transfer* **161**, 120245 (2020).
- ⁴²T. Lee, G. Park, and D. Lee, "Local flow characteristics of subcooled boiling flow of water in a vertical concentric annulus," *Int. J. Multiphase Flow* **28**, 1351–1368 (2002).